01 Jan 1967

An Analytic Model For The Fluxgate Magnetometer

Stanley V. Marshall
Missouri University of Science and Technology

Recommended Citation

S. V. Marshall, "An Analytic Model For The Fluxgate Magnetometer," *IEEE Transactions on Magnetics*, vol. 3, no. 3, pp. 459 - 463, Institute of Electrical and Electronics Engineers, Jan 1967.
The definitive version is available at https://doi.org/10.1109/TMAG.1967.1066078

in the order of $1 \cdot 10^{-5}$. The errors were almost exclusively due to tape deficiencies (dropouts or lumps).

The NRZ format can be used if the data clock and the timing reference of the recorder are synchronous. In this case, the frequency standard represents an error-free data clock in the reproduce process, since the signal is highly time-base corrected with reference to the standard. Since instrumentation recorders are normally available for an analog bandwidth of 6 MHz, they can be used, in the synchronous mode, to record up to 12 Mbit/s serial NRZ. Digitial data at 10 Mbit/s has been recorded and reproduced with excellent signal quality.

A very significant reduction of bit errors can be achieved with the 2-channel version of rotary-head recorders, where eight heads are distributed around the rotating drum so that the recorded tracks of the 2-signal channels are interleaved, and simultaneous information in the two channels is recorded at a distance of about 0.8 inch of track length (45° on a 2-inch diameter drum). The two channels can be used for a full redundancy recording and, if the track of each channel is reduced to 0.005 inch, i.e., one-half of that used in a single-channel recorder, no loss of packing density is incurred. The fact that the two channels are reproduced in a highly time-stable manner makes possible the addition of the two signal channels in the FM mode, before limiting and detection, without producing transients. If a dropout occurs in one channel but not simultaneously in the other, the level of the combined FM carrier drops by 6 dB. This is of no consequence because of the subsequent limiting. The demodulated signal does not vary in amplitude. Since the probability of two dropouts occurring simultaneously in the two channels is extremely small, an error rate of less than $1 \cdot 10^{-8}$ has been achieved.

Digital recording capabilities expected in the near future are based on an 8-channel recorder with 12-MHz bandwidth per channel. Using the redundancy method, four channels at 24 Mbit/s each, i.e., a data stream of 96 Mbit/s, can be recorded with an extremely low error rate, or approximately 200 Mbit/s with moderate error counts.

A digital recorder with very low error rate has an important application when the recording of signals at extremely good SNR is required. Since analog wideband recorders are restricted in their SNR performance, digitizing of such critical information can circumvent this limitation. For instance, at 100 Mbit/s and 10 bits per sample, yielding a SNR of 62 dB rms/rms, an analog bandwidth of 5 MHz can be accommodated.

An Analytic Model for the Fluxgate Magnetometer

STANLEY V. MARSHALL, MEMBER, IEEE

Abstract—**The output voltages from various fluxgate probe types are found to have the same general form, and an analytic model has been developed with which the output may be calculated. In the saturation region where the output pulse is developed, the differential permeability can be closely approximated by an exponential, $dB/dH = k_1 H^{k_2}$, where k_1 and k_2 are on the order of 100 and -2.0, respectively, for cores of Supermalloy or Permalloy 80. Using this model, the effect of the nature of the excitation function on output pulse amplitude and width and the effect of the squareness of the core characteristic can be clearly demonstrated, and good agreement with experimental results has been obtained.**

Introduction

THE FLUXGATE magnetometer, known today as a sensitive field measuring instrument, dates back to the late 1930s or early 1940s. The device was further developed and used during World War II for detection of submarines, and since then has been used extensively in airborne geophysical surveys.[1]–[3] During recent years, it has been used for space exploration.[4] It is the purpose of this paper to present an analytic model for the fluxgate probe as an extension to an analysis begun in an earlier paper.[5] First, to unify the analysis as far as the different probe types are concerned, some various types will be briefly reviewed.

In the first group, the probe element consists of a single rod or tube of high-permeability material about which are wound the excitation and output windings [Fig. 1(a)]. Actually, in practical units, the same winding has been used for both excitation and output.[1] The second harmonic of the output voltage, which is generally used as a measure of the component of the ambient field along the probe axis, is obtained from the total output voltage through filtering.

In the second group, the filtering of odd harmonics is accomplished by connecting the output of two group one probes in opposition[2] [Fig. 1(b)]. A closed core form of this type is the ring-core design[6] [Fig. 1(c)].

In a third group is a probe which is closely related to the mu-metal wire magnetometer with the wire replaced by a hollow tube[7] [Fig. 1(d)]. An excitation winding is wound toroidally around the core and the output winding is circumferentially wound. Cancellation of odd harmonics is accomplished by the orthogonality of the two windings.

It is possible, under certain assumptions, to show that the principle of operation of each probe type is the same, and the analytic model presented applies to either design. The analysis shows that probe sensitivity is related to its geometry and to the shape of the hysteresis loop, and a model is derived which permits quantitative calculations of the output voltage to be made.

Manuscript received March 1, 1967. The work reported in this paper was supported by a NASA Traineeship and is part of a dissertation presented in partial fulfillment of the Ph.D. degree from the University of Missouri, Columbia, Mo.

The author is with the Electrical Engineering Department, University of Missouri, Rolla, Mo.

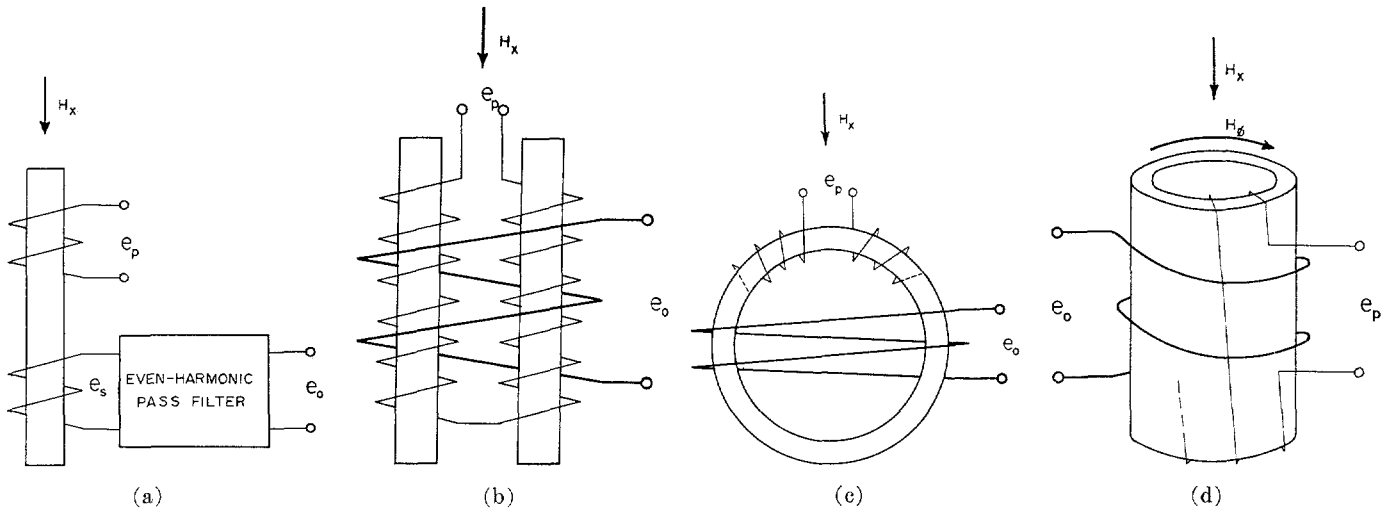

Fig. 1. Fluxgate probe types.

Analysis

For the probe of Fig. 1(a) in the presence of a field H_x, the voltage induced in the secondary due to a periodic excitation voltage e_p of odd symmetry which drives the core well into saturation, twice each excitation period, is

$$e_s = NA(dB/dH)(dH/dt) \times 10^{-8}$$
$$= NA(dH/dt) \times 10^{-8}[(\mu_d)_o + \delta H(\mu_d')_o + \dots] \quad (1)$$

for $0 < t < T/2$, and

$$e_s = -NA(dH/dt) \times 10^{-8}[(\mu_d)_o - \delta H(\mu_d')_o + \dots] \quad (2)$$

for $T/2 < t < T$, where

N —number of output winding turns
A —core area
dH/dt—excitation field
μ_d $= dB/dH$
δH —perturbation in H within the core due to the presence of the ambient field
$(\mu_d)_o$ $= dB/dH$ for $\delta H = 0$
$(\mu_d')_o$ $= d^2B/dH^2$ for $\delta H = 0$.

A perturbation in B is substituted for the perturbation in H giving

$$e_s = NA(dH/dt) \times 10^{-8}\left(\mu_d + \frac{\delta B}{\mu_d}\mu_d' + \dots\right) \quad (3)$$

for $0 < t < T/2$, and

$$e_s = -NA(dH/dt) \times 10^{-8}\left(\mu_d - \frac{\delta B}{\mu_d}\mu_d' + \dots\right) \quad (4)$$

for $T/2 < t < T$. The subscripts of the μ_d and μ_d' terms have been dropped for convenience.

The filter of Fig. 1(a) removes odd harmonics of e_s. By taking one half the sum of corresponding terms of (3) and (4), the result is the even harmonic portion of e_s defined over the entire period. This function is approximated by the first two terms for small ambient fields giving

$$e_o = NA(dH/dt) \times 10^{-8}\frac{\delta B}{\mu_d}\mu_d' \quad (5)$$

for $0 < t < T$.

The dH/dt term is related to the excitation voltage by

$$dH/dt = \frac{e_p \times 10^8}{AN_p\mu_d} \quad (6)$$

where N_p is the number of excitation winding turns, and the perturbation δB may be expressed as

$$\delta B = \mu_a H_x \quad (7)$$

where μ_a is the apparent or effective permeability of the rod-like core to the field H_x.

Substituting (6) and (7) into (5) gives

$$e_o = e_p(N/N_p)\mu_a(\mu_d'/\mu_d^2)H_x$$
$$= e_p(N/N_p)\mu_a F_H H_x \quad (8)$$

where $F_H = \mu_d'/\mu_d^2$.[5]

For the element design of Fig. 1(b) or (c), the odd harmonic filtering is accomplished by the bucking action of the induced voltages on opposite sides of the probe. These induced voltages are given by (3) and (4), and the output is given by (5). If μ_a is defined for each section of the core

$$e_o = e_p(N/N_p)2\mu_a F_H H_x. \quad (9)$$

The apparent permeability is related to the ballistic demagnetization factor K by

$$\mu_a = \frac{\mu_d}{1 + K\mu_d} \quad (10)$$

and when K is small enough, (9) may be written as

$$e_o \doteq e_p(N/N_p)2(\mu_d'/\mu_d)H_x. \quad (11)$$

For a ring-core probe

$$K \doteq 3(\sqrt{A}/M_\ell)^{1.6} \quad (12)$$

where M_ℓ is the core mean length and A is the cross-sectional area.

If for the configuration of Fig. 1(d) the permeability is assumed to be isotropic, the voltage induced in the output coil is

$$e_o = NA(dH_\phi/dt) \times 10^{-8}(dB_x/dH_\phi) \tag{13}$$

and

$$dB_x/dH_\phi = d(\mu_a H_x)/dH_\phi = H_x \frac{\mu_d'}{(1 + K\mu_d)^2}. \tag{14}$$

Substituting (14) into (13) and using (6) gives

$$e_o = e_p(N/N_p)H_x \frac{\mu_d'}{\mu_d(1 + 2K\mu_d + K^2\mu_d^2)}. \tag{15}$$

For cores having large length-to-diameter ratios, (15) differs from (11) only by a factor of two. Thus, under the assumption of isotropy in μ_d, the derived outputs from the three probe types have the same form. The output e_o reaches a maximum when the product of e_p and a nonlinear term in dB/dH reaches a maximum, and the amplitude of the maximum is linearly proportional to the field H_x.

To optimize the sensitivity to H_x, the product $\mu_a F_H$ should be made as large as possible and the excitation function so designed that at the time this maximum is reached, e_p is also a maximum. It can be seen experimentally that the output pulse from a practical probe is formed only after the core is driven into saturation, past what might normally be regarded as the knee of the hysteresis loop. This means that if the analytic model is correct, $\mu_a F_H$ reaches a maximum in the saturation region. It has been observed that the output pulse width is on the order of 10 to 20 μs when the core is excited at frequencies from 0.5 kHz to 1.0 kHz. Then for a reasonably smooth excitation voltage, e_p or dB/dt may be considered constant at the instant the output pulse is formed. Substituting

$$e_p = N_p A \times 10^{-8} dB/dt \tag{16}$$

into (9) gives

$$e_o = 2NA \times 10^{-8}(dB/dt)\mu_a F_H H_x \tag{17}$$

for the time period during which the pulse is formed, and e_o is essentially zero elsewhere. Integrating (17) with respect to time gives

$$\int_{t_i}^{t} e_o dt = 2NA \times 10^{-8} H_x \int_{B_i}^{B} \mu_a F_H dB \tag{18}$$

which shows that the volt-seconds of the output pulse is a constant of the core parameters and H_x, and is independent of the excitation function. That is, one may obtain a large amplitude narrow pulse or a smaller amplitude fatter pulse. Also, (18) shows that following the volt-seconds generated by integration from B_i to $B_{\max}$ during one half-period (assuming the maximum of $\mu_a F_H$ lies within $B_i < B < B_{\max}$), there is another pulse of opposite sign generated when the cycle reverses and integration is from $B_{\max}$ to B_i. The signs of F_H and μ_a do not change, but since the limits on the right-hand integral of (18) are reversed, its sign also changes. The sign for the left-hand integral may change only if e_o changes polarity.

The Model

By plotting experimentally obtained values of dB/dH on log-log coordinate paper, it was found that for Supermalloy and Permalloy 80 over the range from approximately 0.3–3.0 Oe,

$$\mu_d = k_1 H^{k_2} \tag{19}$$

was a reasonable fit to the experimental data. The values of k_1 and k_2 were found to be on the order of 100 and -2.0, respectively.

Substituting (10) and (19) into (9), the output voltage as a function of H is

$$e_o = 2e_p(N/N_p) \frac{k_1 k_2 H^{k_2 - 1}}{k_1 H^{k_2}(1 + K k_1 H^{k_2})} H_x \tag{20}$$

for 0.3 Oe $< H <$ 3.0 Oe. Since e_p is essentially constant during the output pulse, and if the integration is limited to the intervals of t, H, and B within which the main portion of the output pulse is formed,

$$\Delta B = \int_{B_i}^{B} dB = \int_{t_i}^{t} (dB/dt)dt = \int_{H_i}^{H} (dB/dH)dH. \tag{21}$$

For square-wave excitation where saturation occurs at $t = cT$ during the half-period $0 < t < T/2$ and for an arbitrary time interval, (21) gives

$$\Delta t = \frac{\Delta B}{dB/dt} = \frac{cTk_1}{2B_{\max}(k_2 + 1)} (H^{k_2+1} - H_i^{k_2+1}). \tag{22}$$

A time plot of e_o is obtained by substituting

$$e_p = \frac{2N_p A \times 10^{-8} B_{\max}}{cT} \tag{23}$$

into (20) and plotting against values of Δt as computed from (22). The model also gives a pulse for e_o at $t = T/2$ when the square-wave voltage reverses polarity. This pulse is of the same amplitude as the pulse at $t = cT$ but is of opposite polarity.

For a periodic alternating ramp excitation described by

$$\begin{aligned} e_p &= at, && 0 < t < T/2 \\ &= -a(t - T/2), && T/2 < t < T \end{aligned} \tag{24}$$

the voltage at saturation and dB/dt is twice that for the square-wave excitation. Using these values in (20) and (22) gives an output pulse for the alternating ramp excitation that is twice the amplitude and one half the width of that using square-wave excitation. The e_o pulse generated at $t = T/2$ is essentially zero in this case, however, since e_p is essentially zero at this point.

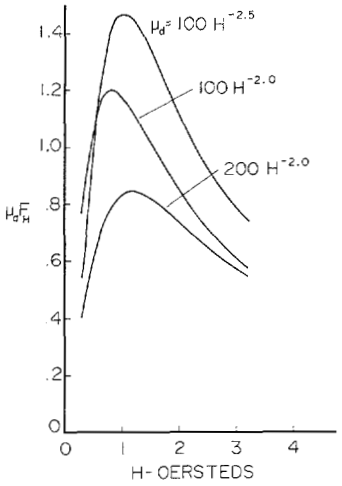

Fig. 2. Calculated relative probe output vs. excitation field for typical Supermalloy or Permalloy 80 ring-cores having demagnetization factors of 0.007.

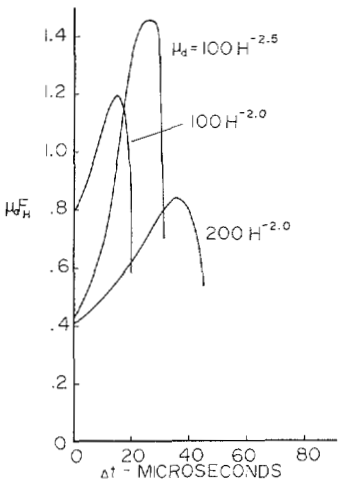

Fig. 3. Calculated time plots of relative probe output for square-wave excitation of 500 Hz.

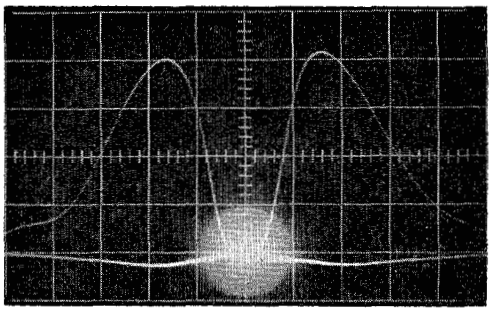

Fig. 4. Measured probe output voltage vs. excitation field for a Supermalloy ring-core with demagnetization factor of 0.007. Vertical: 0.2V/cm; Horizontal: 0.85 Oe/cm, H_x = 0.46 Oe, N_p = 380, N = 100.

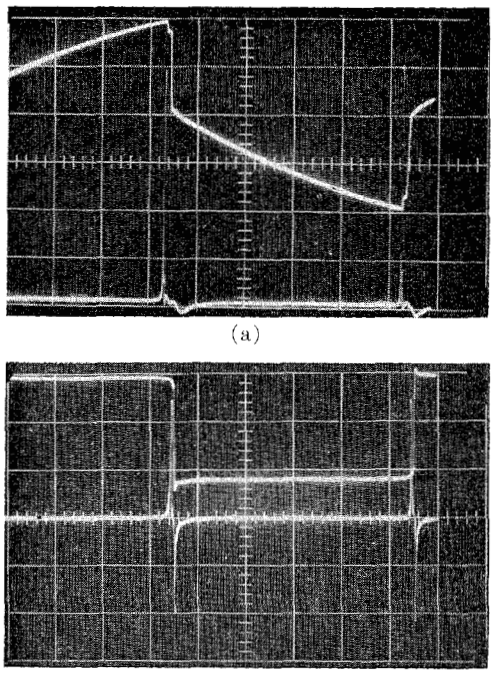

(a) (b)

Fig. 5. Measured probe output voltage for (a) alternating ramp excitation and (b) square-wave excitation. H_x = 0.46 Oe, K = 0.007, N_p = 380, N = 100. Vertical: (top trace) 2V/cm, (bottom) 0.2V/cm; Horizontal: 0.2ms/cm.

Using any excitation function that is not discontinuous just as saturation is entered, (20) and (22) can be used to obtain a time plot of the output pulse by computing e_p and dB/dt at saturation. For such computations, it is convenient to let the initial value of H be 0.3 Oe and calculate at successive values of H differing by a common ratio.

Calculations Based on Model

Calculated plots of the $\mu_a F_H$ term portion of (20) are shown for various values of the parameters k_1 and k_2 chosen to be representative of measured samples of Supermalloy and Permalloy 80 (Fig. 2). A demagnetization factor of $K = 0.007$ was used in the calculations to correspond to the size of ring-core used in the measurements. Practical probes designed for the greatest possible sensitivity would probably have demagnetization factors an order of magnitude smaller than this, and the peak of the $\mu_a F_H$ plot would be correspondingly greater. Time plots of $\mu_a F_H$ were calculated based on a core having a $B_{\max}$ of 7000 gauss driven by a square wave of 500 Hz (Fig. 3). For other frequencies, the pulse amplitude is proportional to frequency and pulse width is inversely proportional to frequency.

To obtain a time plot of e_o for a general excitation function, determine the value of e_p at saturation and substitute this value into (20) to find the maximum of the pulse. The pulse width for the general function is to the pulse width of the Fig. 3 plot as the square-wave saturation voltage is to the saturation voltage of the general function.

The calculated plots show that the output is increased by decreasing k_1 and increasing the magnitude of k_2. That is, the slope of the hysteresis loop should flatten out early and suddenly as a function of H giving a narrow loop having very square knees. Also, implicit in (9) is the dependency of the output amplitude on frequency, output turns, and $B_{\max}$. However, as mentioned before, while operation at higher frequency gives greater output voltage,

the pulse width is correspondingly decreased so that the duty cycle remains the same. Even so, more output pulses are obtained per unit time at the higher frequencies, making it advantageous to operate at as high a frequency as possible.

Experimental Results

An experimental plot to be compared to the calculated plot of Fig. 2 is shown in Fig. 4. This plot of e_o is for a complete excitation cycle using an alternating ramp function shown in Fig. 5(a). In comparing this plot with the calculated plots of $\mu_a F_H$, it is apparent that the measured peak occurs for somewhat larger values of H than was calculated. This is apparently due to the imperfectness of the fit of the exponential curve for μ_d at the beginning of the interval 0.3 Oe $< H <$ 3.0 Oe. The calculated peak of $\mu_a F_H$ obtained from the experimental data is 1.1, which agrees closely with the middle curve of Fig. 2.

The waveforms in Fig. 5(a) and (b) are for 500-Hz excitation where the excitation voltage was adjusted to cause saturation just before the end of each half-period. The pulse widths of the output pulses are roughly one-half that predicted by the model. Again, this discrepancy appears to be due to the sensitivity of the output to μ_d in the early portion of the region 0.3 Oe $< H <$ 3.0 Oe where the model does not fit quite as well as it does near the center of the region.

Conclusion

A model has been presented for the fluxgate probe that agrees well enough with measurements to suggest its value in optimizing probe sensitivity. For maximum sensitivity, the model indicates that in addition to having a large value of B_{max}, the core material should have a narrow hysteresis loop with square corners. Perhaps the chief value in such a model is that selection of core materials can be based on defined core parameters.

Acknowledgment

The author is indebted to Dr. D. L. Waidelich for his encouragement and discussions.

References

[1] E. P. Felch, W. J. Means, T. Slonczewski, L. G. Parratt, L. H. Rumbaugh, and A. J. Tickner, "Air-borne magnetometers for search and survey," *AIEE Trans.*, vol. 66, pp. 641–651, 1947.
[2] R. D. Wyckoff, "The gulf airborne magnetometer," *Geophys.*, vol. 13, pp. 182–208, April 1948.
[3] H. Jensen, "The airborne magnetometer," *Sci. Am.*, vol. 204, pp. 151–162, June 1961.
[4] L. J. Cahill, Jr., "A study of the outer geomagnetic field," *IEEE Trans. Nuclear Science*, vol. NS-10, pp. 10–19, July 1963.
[5] S. V. Marshall, "An analysis of the ring-core fluxgate magnetometer," *Proc. Nat'l Electronics Conf.*, vol. 22, pp. 133–138, 1966.
[6] W. A. Geyger, "The ring-core magnetometer—A new type of second-harmonic flux-gate magnetometer," *Trans. AIEE (Communication and Electronics)*, vol. 81, pp. 65–73, March 1962.
[7] S. C. Ling, "A flux-gate magnetometer for space application," Cornell University Center for Radiophysics and Space Research, Ithaca, N. Y., Quart. Status Rept. to NASA, CRSR 124, NAS Contract NASr-46, June 1, 1962.

A Magnetic Core Analog Memory

FRITZ J. FRIEDLAENDER, SENIOR MEMBER, IEEE, AND JOHN D. McMILLEN, MEMBER, IEEE

***Abstract*—The *stored* flux level in a 50 percent Ni-Fe tape core is read nondestructively to provide an analog memory. The stored flux level is set by means of a low-field ($H < 2H_c$) pulse. This flux level can be read out nondestructively by applying a short high-field pulse ($H > 4H_c$) which produces a peak rate of change of flux proportional to the stored flux level relative to saturation remanence. A subcoercive bias field applied to the core restores it to the original low-field flux state. Experimental data and the model leading to the conception of the memory are presented; and the circuit details of a typical core analog memory are described.**

Manuscript received March 8, 1967. The work reported in this paper was abstracted in part from a Ph.D. dissertation submitted to Purdue University by J. D. McMillen, and was supported in part by the U.S. Army, Navy, and Air Force in the Joint Services Electronics Program under Contract NOOO14-66-COO76-A04.

F. J. Friedlaender is with the School of Electrical Engineering, Purdue University, Lafayette, Ind.
J. D. McMillen is with Industrial Nucleonics Corporation, Columbus, Ohio. He was formerly with Purdue University, Lafayette, Ind.

High-Field Pulsing of a Partially Switched Core

THE PROCESS of high-speed flux reversal in tape cores of 50 percent nickel-iron has been well defined by Bean and Rodbell[1] and by Friedlaender and Leliakov.[2] According to this model, for sufficiently high fields, flux reversal in tape cores of at least ½ to 1-mil thickness initiates at the large tape surface and proceeds through the formation of planar domain walls along the surface of the tape. This action takes place along the entire length of the tape at approximately the same time.

This conclusion has been based upon the analysis of variations of the average flux density in a tape core for various sequences of applied field pulses. Current is driven through a toroidal winding placed on a core to generate the applied magnetic field. A separate toroidal winding is used to observe the rate of change of flux; this signal is termed